

## Article

**Silver Nanoparticle-Mesoporous Oxide Nanocomposite Thin Films: a Platform for Spatially Homogeneous SERS-Active Substrates with Enhanced Stability**

Alejandro Wolosiuk, Nicolas G. Tognalli, Eduardo David Martinez, Mara Granada, María Cecilia Fuentes, Horacio E. Troiani, Sara A. Bilmes, Alejandro Fainstein, and Galo J. A. A. Soler-Illia

ACS Appl. Mater. Interfaces, **Just Accepted Manuscript** • DOI: 10.1021/am500631f • Publication Date (Web): 11 Mar 2014Downloaded from <http://pubs.acs.org> on March 14, 2014**Just Accepted**

“Just Accepted” manuscripts have been peer-reviewed and accepted for publication. They are posted online prior to technical editing, formatting for publication and author proofing. The American Chemical Society provides “Just Accepted” as a free service to the research community to expedite the dissemination of scientific material as soon as possible after acceptance. “Just Accepted” manuscripts appear in full in PDF format accompanied by an HTML abstract. “Just Accepted” manuscripts have been fully peer reviewed, but should not be considered the official version of record. They are accessible to all readers and citable by the Digital Object Identifier (DOI®). “Just Accepted” is an optional service offered to authors. Therefore, the “Just Accepted” Web site may not include all articles that will be published in the journal. After a manuscript is technically edited and formatted, it will be removed from the “Just Accepted” Web site and published as an ASAP article. Note that technical editing may introduce minor changes to the manuscript text and/or graphics which could affect content, and all legal disclaimers and ethical guidelines that apply to the journal pertain. ACS cannot be held responsible for errors or consequences arising from the use of information contained in these “Just Accepted” manuscripts.



# Silver Nanoparticle-Mesoporous Oxide Nanocomposite Thin Films: a Platform for Spatially Homogeneous SERS-Active Substrates with Enhanced Stability

Alejandro Wolosiuk,<sup>a,†</sup> Nicolás G. Tognalli,<sup>b,c,†</sup> Eduardo D. Martínez,<sup>a,†</sup> Mara Granada,<sup>b</sup> M. Cecilia Fuertes,<sup>a,d</sup> Horacio Troiani,<sup>b</sup> Sara A. Bilmes,<sup>e</sup> Alejandro Fainstein<sup>b</sup> and Galo J. A. A. Soler-Illia<sup>a,e\*</sup>

<sup>a</sup> *Gerencia Química - Centro Atómico Constituyentes, Comisión Nacional de Energía Atómica (CNEA), Av. Gral Paz 1499 B1650KNA San Martín, Buenos Aires, Argentina Fax 54-11-6772-7886 Phone 54-11-6772-7032*

<sup>b</sup> *Centro Atómico Bariloche, CNEA, San Carlos de Bariloche, 8400 Argentina.*

<sup>c</sup> *Centro de Innovación Tecnológica, Empresarial y Social (CITES), Sunchales, Santa Fe, Argentina.*

<sup>d</sup> *Instituto Sabato, Universidad Nacional de San Martín - CNEA.*

<sup>e</sup> *DQIAyQF, FCEN, Universidad de Buenos Aires, Ciudad Universitaria, Pabellón II, C1428EHA, Buenos Aires, Argentina*

*E-mail gsoler@cnea.gov.ar*

† These authors contributed equally to this work.

## Abstract

We introduce a nanoparticle-mesoporous oxide thin film composite (NP-MOTF) as low-cost and straightforward sensing platforms for Surface Enhanced Raman Spectroscopy (SERS). Titania, zirconia and silica mesoporous matrices templated with Pluronic®F-127 were synthesized via Evaporation-Induced Self-Assembly and loaded with homogeneously dispersed Ag nanoparticles by soft reduction or photo-reduction. Both methods give rise to uniform and reproducible Raman signals using 4-mercaptopyridine, as a probe molecule. Details on stability and reproducibility of the Raman enhancement are discussed. Extensions in the design of these composite structures were explored including extension to non-thiolated molecules such as Rhodamine 6-G or salicylic acid, patterning techniques for locating the enhancement regions and bilayered mesoporous structures to provide additional control on the environment, and potential size-selective filtration. These inorganic oxide-metal composites stand as extremely simple, reproducible, and versatile platforms for Raman Spectroscopy analysis.

**Keywords:** Surface Enhanced Raman Spectroscopy (SERS); Mesoporous Thin Films; Silver Nanoparticles; Photodeposition; Sensors; Plasmonics

## Introduction

Enhancement of molecular Raman scattering by metallic surfaces opened an exciting research area for single molecule sensing and microscopy, adding new levels of detection not previously envisaged.<sup>1-5</sup> A Surface-Enhanced Raman Scattering (SERS) signal is produced under light excitation of the surface plasmon resonance of metallic nanostructures. The electric field enhancement concentrates in the so called “hot spots”, which are found in gaps between nanoparticles (NPs) in dimers, aggregates, and large fractal structures.<sup>6-8</sup> In addition, certain electronic features of the adsorbed molecule are also required, although the specific mechanism of the chemical contribution to the surface enhancement remains under dispute<sup>9</sup>. Among the metallic surfaces where SERS is observed, silver is the metal of choice because it exhibits a higher scattering cross section which results in larger enhancements. Moreover, tailoring the shape and size of metallic nanoparticles allows a fine tuning of the plasmon absorption which in turn contributes to the enhancement of the Raman signal.

The reproducible preparation of surfaces with a high density of active spots is one of the main current issues regarding SERS active substrates for routine analysis.<sup>3, 10</sup> The reproducible fabrication of this kind of SERS substrates relies mostly on the use of templates that drive NP formation, deposition, and/or synthesis, resulting in ordered arrays of NPs and nanoobjects:<sup>11</sup> alumina anodized oxides membranes, lithography based nanoholes, metal electrodeposition through colloidal templates, nanosphere lithography and self-assembled 2D ordered arrays<sup>12-15,16-17</sup>. The designed platforms should present not only high enhancement factors but also the following issues: i) homogeneity of the enhancement, *i.e.* spot-to-spot reproducibility of the Raman signal,<sup>18</sup> ii) substrate-to-substrate reproducibility, iii) high stability of the nanostructure, and iv) easy and cost-effective preparation and use.<sup>19</sup> As the larger enhancements are produced in hot-spots,<sup>6</sup> an homogeneous distribution of them should be pursued. This is a major challenge since the typical strategies involve either the induced aggregation of Ag or Au NPs from colloidal dispersions, or the fabrication of nanostructured surfaces using high resolution nanofabrication techniques, which present cost and processing limitations for large scale production. Nanoporous systems present an interesting and desirable feature for SERS substrates: the possibility to confer selectivity to the analytes under sensing, either by selective adsorption of molecules or by controlled diffusion across membranes. The fabrication of inexpensive, robust and reproducible SERS active substrates with regular and highly controlled metallic nanostructures included in porous matrices fuels this research area toward real-world environment field data acquisition devices and trace analysis. Recently, several works reported the use of microporous or mesoporous frameworks loaded with metallic NPs as SERS substrates with potential

1  
2  
3 molecular sieving activity.<sup>20-23</sup> In order to project these encouraging systems to real  
4 analytical applications, a broader study concerning the homogeneity, stability,  
5 reproducibility and comparison between different materials is needed.  
6

7 In this work we present the use of mesoporous oxide thin films (MOTF) for  
8 synthesizing Ag SERS active substrates using soft reduction techniques. Titania,  
9 silica or zirconia MOTF were synthesized by Evaporation Induced Self Assembly  
10 (EISA). The precise localization of Ag NPs within the MOTF and the degree of  
11 control of the electroless<sup>24</sup> or photo-induced infiltration<sup>25</sup> lead to the straightforward  
12 fabrication of SERS substrates. This EISA-based preparation is highly attractive  
13 because of the simple experimental setup required and the high control regarding  
14 film homogeneity, mesostructure, pore size and thickness.<sup>26</sup> Soft coating processes  
15 allow film deposition on a variety of surfaces: from flat substrates to complex  
16 systems such as mesoscopic lithographic channels.<sup>27</sup> A fully supported platform  
17 made up of metal NP-mesoporous oxide framework with controlled SERS active  
18 spots would allow connectivity, facilitating the diffusion of analytes along the  
19 supramolecular structure and preventing nanoparticle aggregation. Although recent  
20 work has reported SERS-active MOTF-based materials,<sup>20-21</sup> we present here a  
21 complete study that includes a thorough analysis of the signal intensity and  
22 reproducibility, and its dependence on the NP loading. The influence of particles  
23 formed on the surface, the role of the wafer material and the long-term SERS-active  
24 substrate performance of the nanocomposites are also discussed. These are essential  
25 features in the design of actual analytical applications that so far have not been  
26 addressed in this kind of materials. In addition, the method presented here merges  
27 soft reduction with lithographic patterning, opening the path to combine standard  
28 “*top down*” and “*bottom up*” approaches,<sup>28</sup> aiming at integrated architectures for  
29 advanced sensors.<sup>29, 30</sup> We also demonstrate SERS-active multilayered  
30 mesostructures that can be potentially applied in smart perm-selective membranes,<sup>31-</sup>  
31  
32  
33  
34  
35  
36  
37  
38  
39  
40  
41  
42  
43  
44  
45  
46  
47  
48  
49  
50  
51  
52  
53  
54  
55  
56  
57  
58  
59  
60  
61  
62  
63  
64  
65  
66  
67  
68  
69  
70  
71  
72  
73  
74  
75  
76  
77  
78  
79  
80  
81  
82  
83  
84  
85  
86  
87  
88  
89  
90  
91  
92  
93  
94  
95  
96  
97  
98  
99  
100  
101  
102  
103  
104  
105  
106  
107  
108  
109  
110  
111  
112  
113  
114  
115  
116  
117  
118  
119  
120  
121  
122  
123  
124  
125  
126  
127  
128  
129  
130  
131  
132  
133  
134  
135  
136  
137  
138  
139  
140  
141  
142  
143  
144  
145  
146  
147  
148  
149  
150  
151  
152  
153  
154  
155  
156  
157  
158  
159  
160  
161  
162  
163  
164  
165  
166  
167  
168  
169  
170  
171  
172  
173  
174  
175  
176  
177  
178  
179  
180  
181  
182  
183  
184  
185  
186  
187  
188  
189  
190  
191  
192  
193  
194  
195  
196  
197  
198  
199  
200  
201  
202  
203  
204  
205  
206  
207  
208  
209  
210  
211  
212  
213  
214  
215  
216  
217  
218  
219  
220  
221  
222  
223  
224  
225  
226  
227  
228  
229  
230  
231  
232  
233  
234  
235  
236  
237  
238  
239  
240  
241  
242  
243  
244  
245  
246  
247  
248  
249  
250  
251  
252  
253  
254  
255  
256  
257  
258  
259  
260  
261  
262  
263  
264  
265  
266  
267  
268  
269  
270  
271  
272  
273  
274  
275  
276  
277  
278  
279  
280  
281  
282  
283  
284  
285  
286  
287  
288  
289  
290  
291  
292  
293  
294  
295  
296  
297  
298  
299  
300  
301  
302  
303  
304  
305  
306  
307  
308  
309  
310  
311  
312  
313  
314  
315  
316  
317  
318  
319  
320  
321  
322  
323  
324  
325  
326  
327  
328  
329  
330  
331  
332  
333  
334  
335  
336  
337  
338  
339  
340  
341  
342  
343  
344  
345  
346  
347  
348  
349  
350  
351  
352  
353  
354  
355  
356  
357  
358  
359  
360  
361  
362  
363  
364  
365  
366  
367  
368  
369  
370  
371  
372  
373  
374  
375  
376  
377  
378  
379  
380  
381  
382  
383  
384  
385  
386  
387  
388  
389  
390  
391  
392  
393  
394  
395  
396  
397  
398  
399  
400  
401  
402  
403  
404  
405  
406  
407  
408  
409  
410  
411  
412  
413  
414  
415  
416  
417  
418  
419  
420  
421  
422  
423  
424  
425  
426  
427  
428  
429  
430  
431  
432  
433  
434  
435  
436  
437  
438  
439  
440  
441  
442  
443  
444  
445  
446  
447  
448  
449  
450  
451  
452  
453  
454  
455  
456  
457  
458  
459  
460  
461  
462  
463  
464  
465  
466  
467  
468  
469  
470  
471  
472  
473  
474  
475  
476  
477  
478  
479  
480  
481  
482  
483  
484  
485  
486  
487  
488  
489  
490  
491  
492  
493  
494  
495  
496  
497  
498  
499  
500  
501  
502  
503  
504  
505  
506  
507  
508  
509  
510  
511  
512  
513  
514  
515  
516  
517  
518  
519  
520  
521  
522  
523  
524  
525  
526  
527  
528  
529  
530  
531  
532  
533  
534  
535  
536  
537  
538  
539  
540  
541  
542  
543  
544  
545  
546  
547  
548  
549  
550  
551  
552  
553  
554  
555  
556  
557  
558  
559  
560  
561  
562  
563  
564  
565  
566  
567  
568  
569  
570  
571  
572  
573  
574  
575  
576  
577  
578  
579  
580  
581  
582  
583  
584  
585  
586  
587  
588  
589  
590  
591  
592  
593  
594  
595  
596  
597  
598  
599  
600  
601  
602  
603  
604  
605  
606  
607  
608  
609  
610  
611  
612  
613  
614  
615  
616  
617  
618  
619  
620  
621  
622  
623  
624  
625  
626  
627  
628  
629  
630  
631  
632  
633  
634  
635  
636  
637  
638  
639  
640  
641  
642  
643  
644  
645  
646  
647  
648  
649  
650  
651  
652  
653  
654  
655  
656  
657  
658  
659  
660  
661  
662  
663  
664  
665  
666  
667  
668  
669  
670  
671  
672  
673  
674  
675  
676  
677  
678  
679  
680  
681  
682  
683  
684  
685  
686  
687  
688  
689  
690  
691  
692  
693  
694  
695  
696  
697  
698  
699  
700  
701  
702  
703  
704  
705  
706  
707  
708  
709  
710  
711  
712  
713  
714  
715  
716  
717  
718  
719  
720  
721  
722  
723  
724  
725  
726  
727  
728  
729  
730  
731  
732  
733  
734  
735  
736  
737  
738  
739  
740  
741  
742  
743  
744  
745  
746  
747  
748  
749  
750  
751  
752  
753  
754  
755  
756  
757  
758  
759  
760  
761  
762  
763  
764  
765  
766  
767  
768  
769  
770  
771  
772  
773  
774  
775  
776  
777  
778  
779  
780  
781  
782  
783  
784  
785  
786  
787  
788  
789  
790  
791  
792  
793  
794  
795  
796  
797  
798  
799  
800  
801  
802  
803  
804  
805  
806  
807  
808  
809  
810  
811  
812  
813  
814  
815  
816  
817  
818  
819  
820  
821  
822  
823  
824  
825  
826  
827  
828  
829  
830  
831  
832  
833  
834  
835  
836  
837  
838  
839  
840  
841  
842  
843  
844  
845  
846  
847  
848  
849  
850  
851  
852  
853  
854  
855  
856  
857  
858  
859  
860  
861  
862  
863  
864  
865  
866  
867  
868  
869  
870  
871  
872  
873  
874  
875  
876  
877  
878  
879  
880  
881  
882  
883  
884  
885  
886  
887  
888  
889  
890  
891  
892  
893  
894  
895  
896  
897  
898  
899  
900  
901  
902  
903  
904  
905  
906  
907  
908  
909  
910  
911  
912  
913  
914  
915  
916  
917  
918  
919  
920  
921  
922  
923  
924  
925  
926  
927  
928  
929  
930  
931  
932  
933  
934  
935  
936  
937  
938  
939  
940  
941  
942  
943  
944  
945  
946  
947  
948  
949  
950  
951  
952  
953  
954  
955  
956  
957  
958  
959  
960  
961  
962  
963  
964  
965  
966  
967  
968  
969  
970  
971  
972  
973  
974  
975  
976  
977  
978  
979  
980  
981  
982  
983  
984  
985  
986  
987  
988  
989  
990  
991  
992  
993  
994  
995  
996  
997  
998  
999  
1000

## Experimental

### Film Synthesis

Titania, zirconia and silica MOTF were deposited by dip-coating on glass or silicon substrates at a relative humidity (RH) of 40-50 % for titania or silica and 20% for zirconia. The dip-coating speed used varied between 1-2 mm s<sup>-1</sup>. The detailed preparation techniques have been reported elsewhere.<sup>36-37</sup> ZrCl<sub>4</sub>, TiCl<sub>4</sub> and Si(OEt)<sub>4</sub> were used as the inorganic precursors. Titania precursor solutions were used without aging, and the films were made at 30 °C solution temperature. The composition used

1  
2  
3 was  $\text{TiCl}_4:\text{EtOH}:\text{H}_2\text{O}$  1:40:10. Cetyltrimethylammonium bromide (CTAB) was used  
4 as a template of  $\text{SiO}_2$  films, and Pluronic® F127 block copolymer  
5 ( $\text{HO}(\text{CH}_2\text{CH}_2\text{O})_{106}(\text{CH}_2\text{CH}(\text{CH}_3)\text{O})_{70}(\text{CH}_2\text{CH}_2\text{O})_{106}\text{OH}$ ), for large-pore materials.  
6 After deposition, films were placed in 50% RH chambers for 24 h, and subjected to a  
7 stabilizing thermal treatment procedure consisting of two successive 24 h heat  
8 treatments at 60 and 130 °C, and a final 2 h step at 200 °C. The template was finally  
9 eliminated from all the layers by heating at 350 °C under a still air atmosphere in a  
10 tubular oven, leading to the formation of transparent crack-free thin films.  
11  
12  
13  
14  
15  
16  
17

### 18 **Ag nanoparticle synthesis**

19  
20 Synthesis of Raman active metallic centers in mesoporous oxide matrices  
21 ( $\text{Ag}@\text{MOx}$ ) can be accomplished through electrochemical methods,<sup>38-39</sup> heat post-  
22 reduction synthesis,<sup>40-41</sup> photochemistry<sup>42</sup> or “one pot” synthesis of EISA solutions  
23 precursors and protected nanoparticles.<sup>43</sup> In this context, nucleation and further  
24 growth of metallic seeds are key aspects to control in order to obtain a 3D inverse  
25 metallic framework or a hybrid composite of nanostructured domains of oxide and  
26 metal nanoparticles.<sup>44</sup> Therefore, the pore framework provides an organized array of  
27 fixed size and interconnected nanoreactors for NPs synthesis. The Ag loading of  
28 MOTFs was performed following two different procedures previously developed in  
29 our laboratory: electroless deposition<sup>24</sup> and photo-reduction.<sup>45</sup> All MOTF samples,  
30 with or without Ag NPs, were stored under darkness to avoid photodegradation.  
31  
32  
33  
34  
35

36 **ELECTROLESS DEPOSITION METHOD.** Ag NPs were synthesized within mesoporous  
37 thin films as follows: first, calcined films were immersed in a 1:1 water:ethanol  
38 mixture of  $\text{AgNO}_3$  0.05 M for 15 minutes. Then, 7 % w/w formaldehyde (HCHO)  
39 solution was added until a 1 % w/w final concentration was reached and left under  
40 stirring for 2 hours<sup>24</sup>. After 15 - 20 min a noticeable change in color was observed in  
41  $\text{TiO}_2$  and  $\text{ZrO}_2$  mesoporous films and 6 hours later, a gray silver film was wiped off  
42 from the porous substrate with a tissue paper. In order to obtain Ag deposition in  
43  $\text{SiO}_2$  films, the reducing agent concentration is higher and much longer reduction  
44 times are needed.<sup>24</sup> Alternatively, we employed a  $\text{SnCl}_2$   $10^{-4}$  M / HCl 0.01 M  
45 solution for activation of the silica pores for 10 min.<sup>46</sup>  
46  
47  
48  
49  
50

51 **PHOTO-REDUCTION METHOD.**  $\text{TiO}_2$  mesoporous thin films deposited on silicon  
52 substrates were placed in a plastic container and covered with a 1:1 water:ethanol  
53 mixture of  $\text{AgNO}_3$  0.01 M. After ten minutes in the dark to favour the adsorption of  
54  $\text{Ag}^+$  cations on the pore surface, the container was placed under a UV lamp (355 nm,  
55 15W Phillips black light) for the desired exposure time. An acetate lithography mask  
56  
57  
58  
59  
60

1  
2  
3 was used to pattern the Ag NPs loading.<sup>25</sup> After the Ag infiltration synthesis, the film  
4 surface was gently cleaned with tissue paper wet with ethanol to remove any deposit  
5 formed on the surface of the films. As will be discussed later, the influence of  
6 residual Ag particles on the surface has a significant influence on the SERS  
7 performance.  
8  
9

10  
11  
12 **Molecule adsorption in Ag@MOTF frameworks.** 4-mercaptopyridine (4-MP, Sigma-  
13 Aldrich, 95%), was used as received. Molecule adsorption were prepared as follows. First  
14 the NP-MOTF nanostructures were immersed in ethanol solutions of 10  $\mu\text{M}$ , 50  $\mu\text{M}$  or 250  
15  $\mu\text{M}$  of 4-MP during 30 min. After that, substrates were rinsed with ethanol and finally dried  
16 under a nitrogen gas flow. The same protocol was used in the case of Rhodamine 6G  
17 (incubated from a 7.5  $\mu\text{M}$  solution); adsorption of salicylic acid was performed from 10  
18 mM aqueous solution at pH 6.  
19  
20  
21

22 **Raman measurements.** The enhanced Raman scattered intensity of 4-MP was  
23 measured onto Ag-loaded  $\text{TiO}_2$ ,  $\text{ZrO}_2$  or  $\text{SiO}_2$  samples between  $800\text{ cm}^{-1}$  and  $1300$   
24  $\text{cm}^{-1}$  using a Jobin-Yvon T64000 triple spectrometer operating in subtractive mode  
25 and equipped with a liquid- $\text{N}_2$  cooled charge coupled device. The excitation was  
26 performed with an Ar-Kr ion laser using energies between 1.834 eV (676 nm) and  
27 2.707 eV (458 nm). Typical powers were around 10mW, concentrated on either a  
28  $\sim 100\text{ }\mu\text{m}$  diameter circular spot, or a 7 mm long and  $\sim 100\text{ }\mu\text{m}$  wide line focus. These  
29 were chosen to reduce the photon-induced degradation of the samples. Under the  
30 worst situation (circular spot) the photobleaching was determined to be around 5 %  
31 after 120 s of data acquisition (Supporting Information, fig. S1).  
32  
33  
34  
35  
36  
37  
38

### 39 **Film characterization**

40 **SMALL ANGLE X-RAY SCATTERING (SAXS) AND X-RAY REFLECTOMETRY (XRR).**  
41 Film mesostructures were analyzed using Small Angle X-ray Scattering (SAXS) at  
42 the D11A-SAXS2 line of LNLS ( $\lambda = 1.608\text{ \AA}$  or  $1.488\text{ \AA}$ ) at normal and  $3^\circ$  incidence  
43 and a MARCCD 2D detector. Films thickness and density were obtained from X-ray  
44 Reflectometry (XRR) measurements performed at the D10A-XRD2 line of  
45 Laboratório Nacional de Luz Síncrotron, Campinas, SP, Brazil ( $\lambda = 1.5498\text{ \AA}$ ). In  
46 order to obtain accurate film density values, the critical angle measurements were  
47 performed at low humidity, to avoid atmospheric water condensation within the  
48 pores that leads to underestimation of mesoporosity. Data and model analysis is  
49 described in a previous work<sup>24</sup>.  
50  
51  
52  
53

54 **ELECTRON MICROSCOPY (TEM AND SEM).** TEM images were obtained from a CM  
55 200 Philips high-resolution transmission electron microscope equipped with an ultra  
56 twin objective lens and an acceleration voltage of 200 kV (CAB - CNEA). Samples  
57  
58  
59  
60

1  
2  
3 were obtained by scratching the Ag@MOTF films from the substrate and deposited  
4 on carbon coated copper grids. Field emission-scanning electron microscopy (FE-  
5 SEM) images were obtained with a ZEISS LEO 982 GEMINI field emission  
6 electron microscope using an in-lens detector to improve resolution.  
7

8 **OPTICAL CHARACTERIZATION.** UV/Vis spectra were obtained employing a Hewlett-  
9 Packard 8453 spectrophotometer in transmission mode; films were deposited on  
10 microscope glass slides. The thickness and the optical constants  $n(\lambda)$  and  $k(\lambda)$  of  
11 MOTF or NP-MOTF were characterized by ellipsometry in a commercial SOPRA  
12 GES5 multispectral ellipsometer in microspot configuration; ellipsometry data was  
13 analyzed with Winelli II (Sopra). Film porosity was determined by spectrometric  
14 ellipsometry while varying the water vapor pressure in a controlled humidity  
15 chamber, according to Boissiere et al.<sup>47</sup>  
16  
17  
18  
19  
20  
21  
22  
23

## 24 Results and discussion

### 25 Ag nanoparticle synthesis in MOTF

26  
27  
28 The synthesis procedures used to load Ag NPs inside SiO<sub>2</sub> and TiO<sub>2</sub> MOTFs were  
29 presented in detail in previous works.<sup>24-25</sup> Here, we have extended the synthesis of  
30 infiltrated Ag NP to the case of ZrO<sub>2</sub> MOTF for which similar trends are obtained.  
31 Figure 1a shows the absorption spectrum of ZrO<sub>2</sub> film templated with a triblock  
32 copolymer non-ionic surfactant (Pluronic® F-127) deposited on glass and after 5,  
33 15 and 120 minutes of reaction in the AgNO<sub>3</sub>/HCHO mixture. As a result of the  
34 nucleation and growth of Ag NPs, a plasmon band develops as shown in Figure 1a.  
35 A clear trend is visible showing a progressive increase in the band intensity and a  
36 red-shift (from 440 nm to 480 nm). This can be qualitatively attributed to the  
37 increase in the number of particles, their size, and their plasmon interactions, as was  
38 demonstrated for Au@TiO<sub>2</sub> MOTF.<sup>48</sup> In order to obtain a quantitative view, the  
39 filling process in ZrO<sub>2</sub> and TiO<sub>2</sub> thin films has been followed using X-ray  
40 reflectivity (XRR), and Energy Dispersive X-Ray scattering (EDX).<sup>24, 49</sup> As time  
41 evolves, the fraction of Ag synthesized inside the pores increases, reaching a  
42 maximum pore filling of around 45% in the case of TiO<sub>2</sub> based films (Supporting  
43 Information Figure S2) and 18% in the case of ZrO<sub>2</sub> after 2h of reaction (Figure 1b).  
44  
45  
46  
47  
48  
49  
50  
51  
52  
53  
54  
55  
56  
57  
58  
59  
60

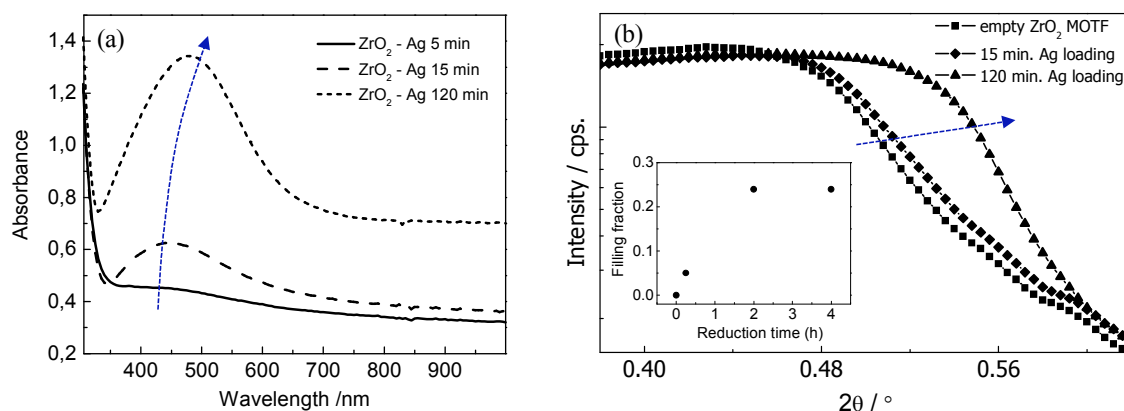


**Figure 1.** a) Absorption spectra of Ag@ZrO<sub>2</sub>-F127 composite films synthesized by electroless reduction with different reduction times. The blue arrow indicates the evolution of the plasmon resonance. b) XRR curves for Ag@ZrO<sub>2</sub>-F127 with different electroless reduction times. The arrow indicates increasing time. Inset: time evolution of the pore filling fraction with Ag NP, calculated from XRR critical angle.

Figure 2 shows TEM images of Ag@ZrO<sub>2</sub> MOTF composite films after 5 and 120 minutes of reaction. These films present mesostructures derived from cubic *Im3m* or *Fm3m* uniaxially distorted after thermal treatment according to SAXS and TEM. After AgNO<sub>3</sub> chemical reduction, uniform Ag particles are embedded within the ZrO<sub>2</sub> matrix pores, and are visualized as dark spots ~ 8-10 nm diameter, in good agreement with the known pore dimensions of F127-templated MOTF. The mesoporous host limits the Ag NPs size but not the distribution within the templated mesostructure. SAXS of samples after reduction, performed at 90° incidence show a diffraction ring corresponding to the  $d_{110}$  distance of an *Im3m* mesostructure located at 131 Å ( $a=18.5$  nm), pointing out that the mesopore structure remains intact after Ag synthesis (inset in Figure 2a).



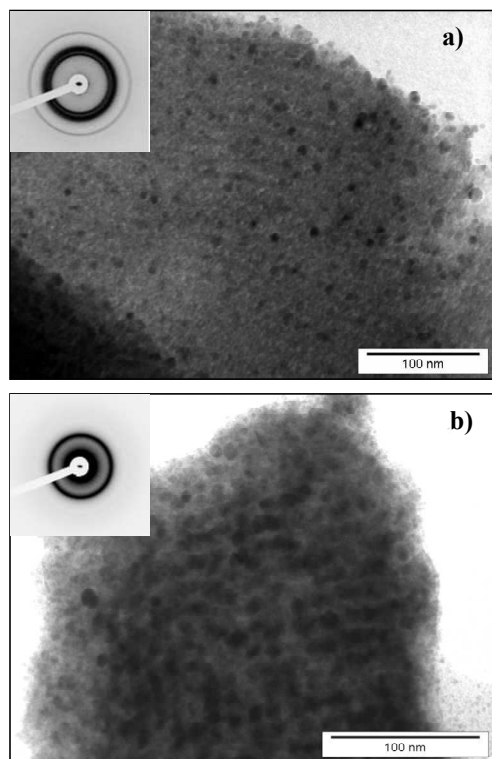


**Figure 2.** TEM micrographs of Ag@ZrO<sub>2</sub> mesoporous films at different Ag NP synthesis stages after: (a) 5 min, (b) 2 hours.

When increasing the electroless deposition time (Figure 2b), a higher density of homogeneously distributed Ag NPs along the mesoporous matrix is observed. SAXS also shows that the mesoporous structure long range is preserved when small doping of particles is analyzed. For longer reduction times, Ag loading within the mesopores becomes higher and two features are observed (insets in Figure 2a and 2b): a diffuse scattering due to the higher NPs content appears at low  $q$  values, and the intensity of the  $d_{110}$  diffraction signal decreases, due to an increase in the average electronic density of the pores that decreases in turn the scattering contrast between pore and inorganic walls. Although the NPs are not forming an ordered array, a careful observation of the TEM data shows that they are homogeneously distributed along the MOTF samples.<sup>24</sup>

### SERS signal in Ag@ZrO<sub>2</sub> MOTF matrices

After 4-MP ( $C_{2v}$  molecule) adsorption in the NP-MOTF films, Raman signals clearly show up in a series of spectra with different loading of Ag NPs (Figure 3a). For nanocomposite films produced after very short reduction times, no distinguishable

1  
2  
3 features are observed and the spectra are characterized by a large background with  
4 broad features. For longer reduction times, the Ag NPs loading increases, and clear  
5 and intense Raman lines develop, accompanied by a steady decrease of the  
6 background. The bands around  $1100\text{ cm}^{-1}$  and  $1008\text{ cm}^{-1}$  are associated with the ring  
7 breathing and the C-S stretching mode of the molecule, while at  $1210\text{ cm}^{-1}$  the  
8 characteristic  $\beta_{\text{(CH)}}$  mode of 4-MP is observed.<sup>50</sup>

9  
10  
11 Figure 3b shows the intensity profile of the  $1100\text{ cm}^{-1}$  Raman signal of 4-MP as a  
12 function of the laser excitation wavelength for the Ag@ZrO<sub>2</sub> substrates with  
13 increasing Ag loading time. The three Raman profiles display a maximum signal at  
14 around  $\sim 500\text{ nm}$ ; a slight shift to longer wavelengths can be observed as the Ag NP  
15 filling increases. The wavelength interval of the signal increase agrees well with the  
16 plasmon resonance of isolated Ag nanoparticles (cf. the absorption spectra shown in  
17 Figure 1a). In addition, a Raman intensity tail towards longer wavelengths is also  
18 observed, which becomes a shoulder around  $\sim 550\text{ nm}$  as the Ag loading increases.  
19 This region of the spectrum is typical of plasmon modes due to interacting particles,  
20 as discussed in our previous work.<sup>48, 51-53</sup> The observed correlation between the  
21 plasmon resonances and the increase of the observed signal strongly suggests that  
22 the confined Ag NP are responsible of this Raman enhancement.  
23  
24  
25  
26  
27  
28  
29  
30  
31  
32  
33  
34  
35  
36  
37  
38  
39  
40  
41  
42  
43  
44  
45  
46  
47  
48  
49  
50  
51  
52  
53  
54  
55  
56  
57  
58  
59  
60

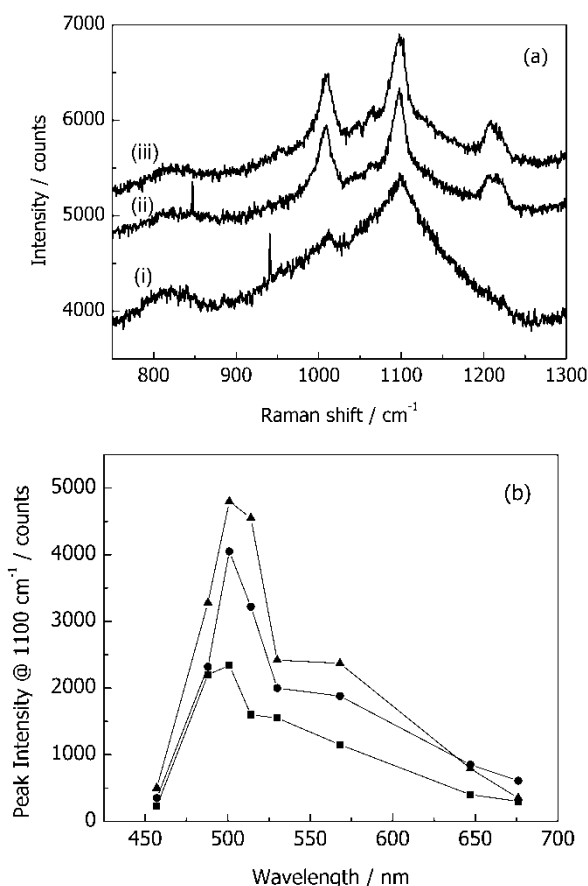


**Figure 3.** a) 4-MP Raman spectra in Ag@ZrO<sub>2</sub> MOTF deposited on glass after AgNO<sub>3</sub>/HCHO electroless deposition increasing reaction times: (i) 5 min, (ii) 15 min and (iii) 120 min. b) Raman intensity profile of the 4-MP signal as a function of the laser excitation wavelength for the Ag@ZrO<sub>2</sub> MOTF after: (■) 5 min, (●) 15 min and (▲) 120 min of electroless deposition. Lines are for eye guidance only.

### Raman excitation profiles for different MOTFs

Figure 4 compares the Raman spectra for different SERS-active substrates. Nanocomposites Ag@TiO<sub>2</sub> and Ag@ZrO<sub>2</sub> matrices show almost the same spectra as a mechanically roughened Ag surface, with slightly lower intensities.

As previously mentioned, an important factor for the development of an analytical platform for SERS enhanced signals is the requisite to have a reproducible and spatially homogeneous signal.<sup>3, 10</sup> In this work, a SERS signal was always observed when Ag NPs were synthesized inside the pores of different MOTFs. As shown in Figure 5, the dependence of the Raman intensity signal with laser excitation wavelength measured at 1100 cm<sup>-1</sup> shows similar behaviour for the MOTF studied

but, with peak location and broadness dependent on the mesoporous oxide matrix used.

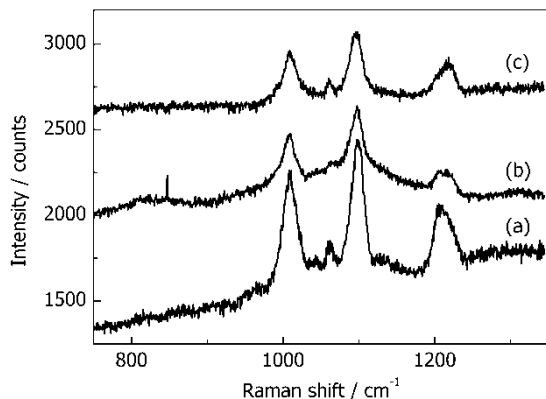


**Figure 4.** 4-MP Raman spectra measured over different systems (a) mechanically roughened Ag, (b) Ag@ZrO<sub>2</sub> MOTF and (c) Ag@TiO<sub>2</sub> MOTF. The samples were excited with a laser at 568.1 nm with 10 mW output and 30 seconds of acquisition time. 4-MP was adsorbed from a 0.25 mM solution.

Control experiments in empty MOTFs gave only background signals (see Supporting Information Figure S3) whereas metal NPs assembled over non mesoporous frameworks or Ag roughened foils gave highly non-uniform signals, as shown previously.<sup>50</sup>

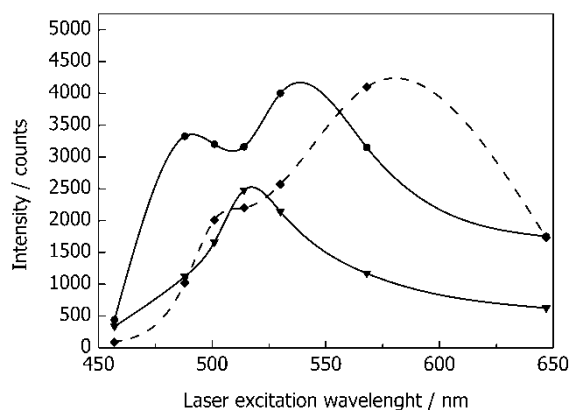


**Figure 5.** Raman intensity signal at 1100 cm<sup>-1</sup> with variable wavelength laser excitation for different Ag@MOTF: (▼) Ag@ZrO<sub>2</sub>, (◆) Ag@TiO<sub>2</sub> and (●) Ag@SiO<sub>2</sub>. Lines are for eye guidance only.

### SERS signal uniformity in Ag@MOTF

AgNP-MOTF matrices show a remarkably homogeneous spatial distribution of Raman intensities within 10% of signal dispersion in a 1 mm<sup>2</sup> area as shown in Figure 6 for various matrices. This is a promising result in terms of a reproducible platform for analytical determinations.<sup>19</sup> Recent work has reported 5-6% standard deviation in the pentachlorophenol SERS signal obtained on cysteamine-modified silver nanoparticle aggregates.<sup>54</sup> The route presented here permits to select among a choice of MOTF tailored for specific applications, or for further chemical surface pore modifications; detailed studies are underway.

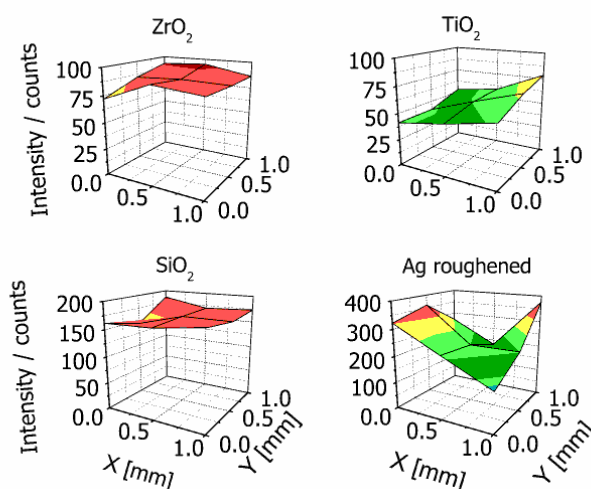


**Figure 6.** 1100 cm<sup>-1</sup> 4-MP Raman signal maps of Ag@O<sub>2</sub> MOTF substrates studied in a 1 x 1 mm<sup>2</sup> area. Spots were measured every 0.5 mm using a 10 mW 514.5 nm laser line focused on a 100 μm circular spot. Acquisition time was 10 seconds. 1100 cm<sup>-1</sup> signal averages are Ag@ZrO<sub>2</sub> (86±6), Ag@TiO<sub>2</sub> (60±10), SiO<sub>2</sub> (170±10) and roughened Ag (260±70).

As no signal is detected in the unloaded MOTFs, even after long acquisition times and higher 4-MP concentration, it was not possible to calculate an enhancement factor (EF); however, the similar intensity compared to Ag roughened substrates, which are typically characterized by EF on the order of 10<sup>3</sup> - 10<sup>5</sup>, makes us estimate comparable values for our systems.<sup>55-56</sup> It is worth noting that the EISA approach presented here facilitates an easy substrate platform production and surface

1  
2  
3 modification for SERS detection with the additional advantage of signal  
4 reproducibility. Other SERS substrates have been reported with higher enhancement  
5 factors but only after a sequence of complex steps or only on specific templates. In  
6 the following sections we will address the rational design of a TiO<sub>2</sub> MOTF platform  
7 that benefits from a photochemical strategy in order to localize the Ag NPs, and  
8 hence the Raman enhancement, and to generate uniform Raman spectra across the  
9 whole SERS surface substrate.  
10  
11  
12

### 13 14 15 **SERS effect in TiO<sub>2</sub> MOTF with photodeposited Ag NPs**

16 Photodeposition of Ag NPs using UV photochemistry<sup>57</sup> opens the possibility to use  
17 conventional photolithography masks in order to transfer a pattern and therefore  
18 localize the regions of SERS enhancement. The photoreduction (PR) process for  
19 loading the mesoporous titania films with Ag NPs has some advantages compared to  
20 the electroless deposition method. For instance, the intensity of the UV light and the  
21 exposure time can be easily controlled. On the other hand, the stirring conditions  
22 during the electroless deposition method can have a significant effect in the  
23 homogeneity of the Ag NP loading, especially for large sample areas.  
24  
25

26 Ag NP synthesis within TiO<sub>2</sub> MOTF using the PR approach also results in  
27 homogeneously filled systems. Ellipsometric optical properties of the Ag@TiO<sub>2</sub>  
28 MOTF deposited on Si substrates are characterized by broad absorption spectra in  
29 the 500 – 700 nm range (see Supporting Information, Figure S5). Again, close  
30 contact between Ag NP within the MOTF results in plasmon interactions affecting  
31 the observed spectra. Saturation filling fractions with Ag NP obtained by this  
32 method (~55 % of the total pore volume) are consistent with previous works.<sup>25, 45</sup>  
33 Nonetheless, the PR approach is highly dependent on the photocatalytic properties of  
34 the TiO<sub>2</sub> anatase phase ( $E_g \sim 3.2$  eV). The crystalline nature of the mesoporous film  
35 depends in turn on the film substrate and the thermal treatment applied.<sup>58-59</sup> The  
36 efficiency of Ag<sup>+</sup> photo-reduction was found to be optimal (higher loading fraction  
37 at equal irradiation doses) when TiO<sub>2</sub> MOTFs are deposited on silicon instead of  
38 glass. The influence of the substrate on the PR method and the derived SERS effect  
39 is shown in the Supporting Information (Figure S4) where two kind of glasses,  
40 borosilicate (Pyrex®) and soda-lime glass, were used in comparison with silicon.  
41 The photocatalytic nature of this method makes SiO<sub>2</sub> based MOTFs inert for this  
42 process. ZrO<sub>2</sub> MOTF display however a less efficient but noticeable Ag<sup>+</sup> photo-  
43 reduction performance.  
44  
45  
46  
47  
48  
49  
50  
51

52 The SERS signals observed for PR processed NP-MOTF composites are intense and  
53 homogeneous along the substrates, as will be discussed in detail below in the case of  
54 4-TP. Interestingly, when Rhodamine 6G and salicylic acid are put in contact with  
55 the SERS-active nanocomposite, intense SERS spectra are obtained, demonstrating  
56 that the molecules are in close proximity or even adsorbed onto the trapped Ag NP,  
57  
58  
59

and can be detected (SI, Figure S6). Ongoing experiments are aimed at assessing whether these molecules are adsorbed onto the titania or the silver surface.

### Patterning the SERS effect

Figure 7 shows an example of the ability of the PR method to localize the SERS effect in an F127-templated TiO<sub>2</sub> MOTF deposited on silicon. The photolithography process was applied using an acetate mask with a pattern consisting in 1 mm side transparent squares, 1 mm spaced. The UV exposure time was 120 minutes, giving a filling fraction of (40 ± 5)% of the total porous volume of the film (45%). After the incubation of 4-MP the Raman signal was acquired in different points of the sample shown as white dots in the upper picture of Figure 7.

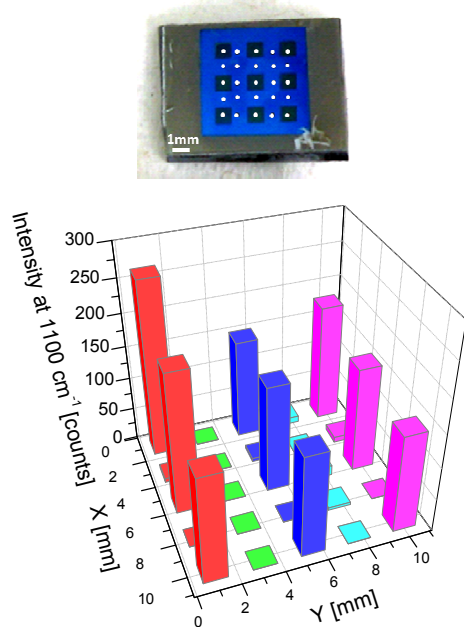


**Figure 7:** Raman intensity profile measured from the 4-MP peak intensity at 1100 cm<sup>-1</sup> in F127-templated TiO<sub>2</sub> on silicon substrate, loaded with Ag NPs by PR method after 120 minutes of UV exposure with the use of a lithographic mask. Spectra obtained using 514.5 nm, 20 mW, 10s. On top, optical image of the patterned sample showing in grey/blue the areas loaded/unloaded with Ag NPs; in white, the spots where the Raman spectrum of 4-MP was measured.

The intensity of the Raman signal, reported as the height in the main peak of 4-MP at 1100 cm<sup>-1</sup>, is clearly dependent on the measurement spot, obtaining a noticeable Raman signal from the spots loaded with Ag. In addition, the spatial homogeneity of the Raman signal spans across the millimeter scale. The standard deviation of the signal homogeneity for the systems so far prepared is in the order of 20%, which can be attributed to the optics system used for the patterning (UV lamp and polymer

masks), which are not yet optimized. However, Figure 7 shows the potential of NP-MOTF nanosystems to be integrated in lab-on-chip architectures that combine “bottom-up” with “top-down” strategies.

Substrate-to-substrate Raman signal repeatability is a fundamental issue that also needs to be satisfied in analytical methods.<sup>19</sup> Figure 8A shows the 4-MP Raman spectra of TiO<sub>2</sub> MOTF samples pertaining to independent synthesis batches. All samples were loaded with Ag NPs using the PR method with a 30 minutes UV exposure (metal filling fraction =  $23 \pm 3\%$  of total porosity), then exposed to 4-MP and stored in the dark. The high reproducibility of the signals is evident (substrate-to-substrate standard deviation in the order of 10%), confirming that the method is highly reproducible and potentially scalable to real applications. When the nanocomposite substrates were stored in plastic bags under mild humidity and kept in the dark, the plasmonic properties did not change, and reproducible SERS signals could be obtained on substrates stored for periods of several months. This stability is greatly enhanced in the case of substrates exposed to thiol-containing analytes. Figure 8B shows the spectra of 4-MP loaded samples stored in the dark for periods up to 42 months. It can be observed that the signal variation is within 10% of the original signal, demonstrating that these NP-MOTF composites are extremely stable and can retain the analytes for long periods with no significant signal variations. This exceptional stability in the presence of thiol-containing molecules can be ascribed to a surface stabilization by thiol groups.

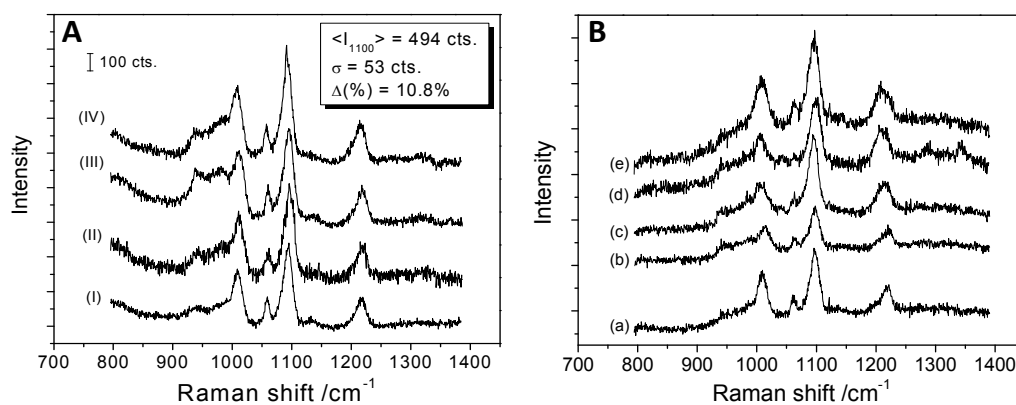


**Figure 8:** Raman spectra of 4-MP in Ag@TiO<sub>2</sub> MOTF/silicon loaded with Ag NPs by PR method after 30 minutes of UV exposure. A: measurements performed on different substrates, measured after preparation. B Measurements performed on independent substrates prepared in different occasions. The elapsed time (in months) between preparation and measurement were (a) 0, (b) 1, (c) 5, (d) 23, and (e) 42 months.



### Ag surface particles on Ag@TiO<sub>2</sub> MOTF

In the electroless deposition and photodeposition methods reported here, it is possible to obtain highly controlled Ag NPs within the mesoporous matrix. However, depending on the synthesis or aging conditions, Ag NPs can be present at the surface of the porous oxide framework, which changes the SERS signal. As stated in the Experimental section, a cleaning procedure is always applied after the synthesis of Ag NPs with any of the methods previously discussed. In this section we will analyze the influence of the surface deposited Ag NP particles on the SERS spectrum.

FE-SEM micrographs of different regions of the MOTF topmost surface after the photolithographic Ag NP synthesis are compared in Figure 9. As expected, right below the dark zones of the photolithographic mask, no Ag NPs on the mesoporous film surfaces are detected (Figure 9a). On the other hand, in Figure 9b the TiO<sub>2</sub> surface under the transparent region of the mask shows a monodisperse distribution of Ag NPs with sizes comparable to the MOTF pore size (~10 nm). Clearly in Figure 9c, a different result is seen when no lithography mask is used. In that case, larger particles of irregular shapes (faceted, triangular plates and rods) and smaller particles in very close contact covering the MOTF surface are observed.

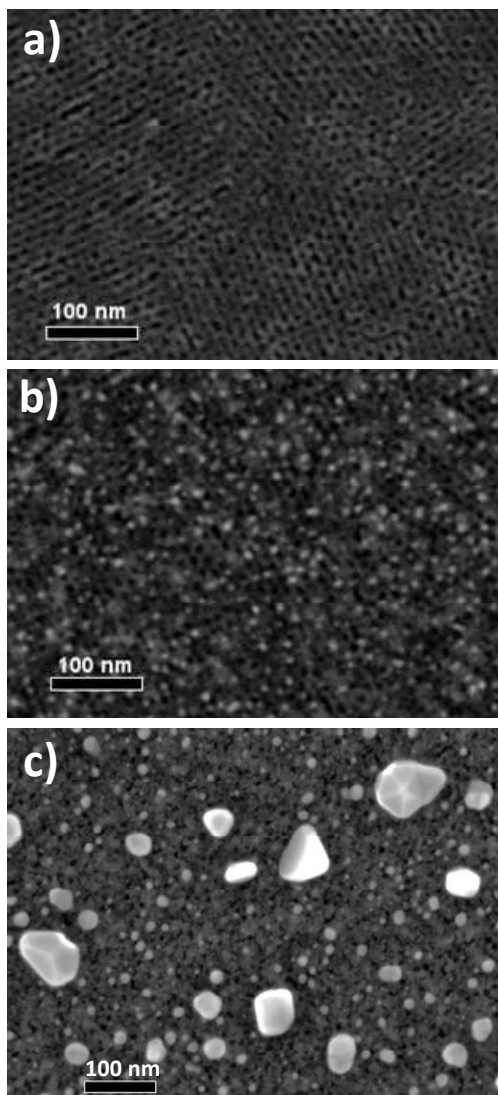
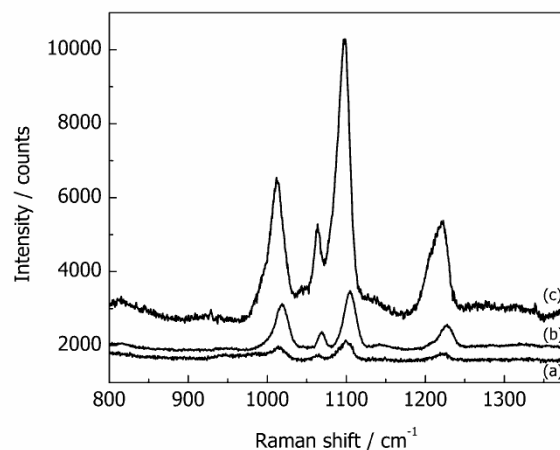


**Figure 9:** FE-SEM images of  $\text{TiO}_2$ -F127/silicon loaded with Ag by PR method using a photolithography mask ( $t_{UV}=30$  min). In a) the surface state under the dark zone of the mask, in b) the surface under the transparent zone, in c) the surface in the uncovered region of the sample.

41  
42  
43  
44  
45  
46  
47  
48  
49  
50  
51  
52  
53  
54  
55  
56  
57  
58  
59  
60

These Ag surface particles have an important influence on the Raman signal enhancement, as shown in Figure 10. In the absence of any photolithographic mask and no cleaning, where the surface of the MOTF is directly exposed to the silver precursor solution, very intense Raman signals are obtained (Figure 10a). However, the SERS effect strongly depends on the measurement location due to the inhomogeneous distribution of Ag particles and the resulting “hot spots” on the MOTF surface. In contrast, Raman enhancements in the regions that were exposed to

1  
2  
3 UV light under the transparent regions of the mask are 3 to 5 times lower, whether or  
4 not the surface is cleaned (Figures 10b and 10c). Again, only after cleaning with a  
5 tissue paper, a reproducible although less intense spectrum is obtained across the  
6 Raman active film.  
7  
8



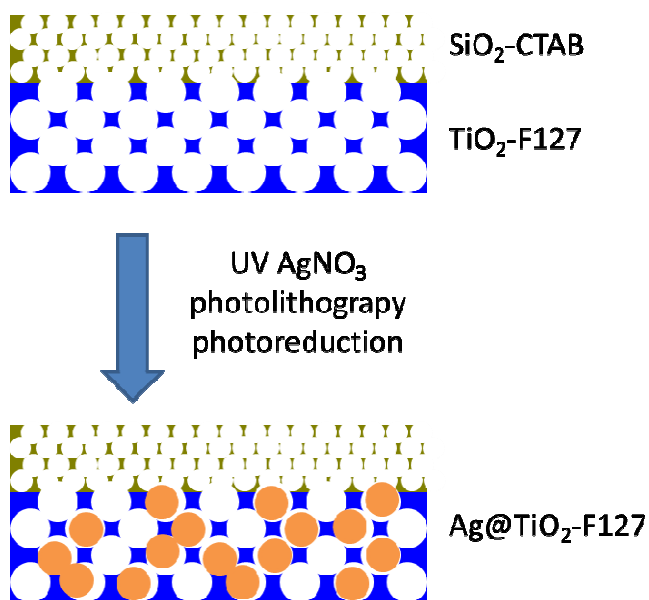
27  
28 **Figure 10:** Raman spectra of 10  $\mu\text{M}$  4-MP adsorbed in Ag@TiO<sub>2</sub> MOTF/silicon by  
29 the PR method: (a) photolithographic mask and performing a surface cleaning, (b)  
30 photolithographic mask and no surface cleaning step, and (c) no photolithographic  
31 mask and no surface cleaning. In all cases UV illumination time for Ag NP synthesis  
32 was 30 min. Laser excitation wavelength was 514.5 nm, 20 mW. Signal was  
33 acquired twice for 60 seconds and averaged.  
34  
35

36  
37 It is worth to mention that although the intensity of the signal is almost one order of  
38 magnitude higher in the samples presenting surface nanoparticles than in the cleaned  
39 samples, those high signals are quite inhomogeneous throughout the film surface.  
40 Therefore, if an analytical technique is to be developed, there will be a trade-off  
41 between high signal intensity and reproducibility.<sup>19</sup> This effect has been recently  
42 reported in yolk-porous shell nanocomposite colloids, and an extra purification step  
43 was deemed as a necessary step towards a predictable functionality for SERS-active  
44 nanomaterials.<sup>60</sup>  
45  
46  
47

### 48 49 **SERS effect in bilayered mesoporous structures**

50  
51 A photochemically non-reactive SiO<sub>2</sub> mesoporous layer was deposited on top of a  
52 nanoparticle-loaded mesoporous titania thin film. Previous works demonstrated that  
53 Ag<sup>+</sup> can be selectively photoreduced within the TiO<sub>2</sub> layer in silica-titania bilayer  
54 MOTF, leading to vertical positioning of NP due to chemical selectivity.<sup>25</sup> With the  
55 addition of the photopatterning procedures, the extension to 3D localization is  
56  
57  
58  
59

straightforward. The presence of a top mesoporous film with controllable pore size and surface chemistry would allow the diffusion of the SERS analyte while excluding the presence of superficial inhomogeneous hot spots and Ag NP, which is an important issue regarding the reproducibility of SERS measurements as demonstrated above. Apart from resolving the “particle on surface” problem by avoiding their formation, since no nucleation takes place on SiO<sub>2</sub>, an empty mesoporous overlayer represents an opportunity for the control of the selectivity in analyte detection, as mesoporous SiO<sub>2</sub> MOTF (upper layer) can be tuned both in its pore size and its surface functionality, acting as porous permselective membranes (see Scheme 1).<sup>25,26</sup> Recently, López-Puente et. al demonstrated that mesoporous thin films can act as molecular sieves, allowing selective diffusion and detection of small molecules in biological mixtures.<sup>20</sup>



**Scheme 1.** Schematic representation of a bilayered MOTF with a SiO<sub>2</sub> MOTF templated with CTAB over a TiO<sub>2</sub> MOTF templated with Pluronic® F127. Ag NP synthesis occurs only in the TiO<sub>2</sub> MOTF layer.

Figure 11 shows the Raman spectra of 4-MP on a bilayer structured sample comprising a SiO<sub>2</sub>-CTAB layer (103 ± 4 nm thick) deposited over a TiO<sub>2</sub>-F127 (110 ± 5 nm thick) and loaded with Ag NPs by PR after 120 minutes of UV exposure using a photolithographic mask.

In this kind of bilayer structures, the areas of the samples covered and uncovered with the photolithography mask display almost identical signal without any surface cleaning, showing the efficiency of the SiO<sub>2</sub> layer in avoiding Ag particle formation. This experiment demonstrates that the Ag NP embedded within the TiO<sub>2</sub> MOTF give rise to the Raman spectrum observed, even if they are “buried” in a multilayer.

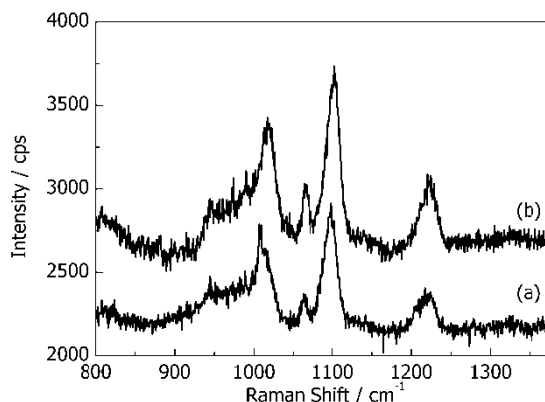


**Figure 11.** Raman spectra of 10  $\mu\text{M}$  4-MP adsorbed in (a) bilayer SiO<sub>2</sub>-CTAB/Ag@TiO<sub>2</sub> MOTF/silicon and (b) Ag@TiO<sub>2</sub>-MOTF/silicon. Both systems were loaded with Ag NPs using the PR method with a lithographic mask and 120 minutes of UV exposure. Laser excitation wavelength was 514.5 nm, 20 mW output power. Signal was acquired twice for 60 seconds and averaged.

## Conclusions

In summary, we have demonstrated a reproducible and simple substrate platform based on mesoporous oxide thin films containing Ag NP for SERS chemical analysis. Reproducible Raman-active nanocomposite substrates have been obtained on TiO<sub>2</sub>, SiO<sub>2</sub> and ZrO<sub>2</sub> MOTFs. Raman signals are well-defined and uniform in the sub-millimeter scale across centimeter-sized substrates. The different oxide frameworks are high  $k$ -dielectric, optically transparent and provide specific surface chemistries with characteristic properties: photocatalysis (TiO<sub>2</sub>), tunable surface silane chemistry (SiO<sub>2</sub>) and resistance to harsh chemical conditions (ZrO<sub>2</sub>). It has been demonstrated that these MOTF can be modified by adding a wide variety of nanoparticulate, organic or polymeric modifiers.<sup>61</sup> This broad palette of metal NP supporting materials opens the possibility for specific SERS substrates with tailored properties and functions in an integrated chemical device. The modulation of the NP surface plasmon absorption using different MOTF matrices and pore sizes tunes SERS intensity and wavelength selectivity.<sup>48</sup> In addition, bilayer structures and

1  
2  
3 photolithography provide additional freedom in the design of functional plasmon  
4 based sensors by locating the Ag loading.

5  
6 The obtained SERS enhancements observed here are not spectacular, but we have to  
7 stress that they are extremely reproducible, that the NP-MOTF Raman signals are  
8 exceptionally stable along time, and that the substrates are easy to prepare through a  
9 highly reproducible and low-cost method that permits to process large surfaces. All  
10 these factors intervene in the overall performance of a nanostructured substrate.<sup>19</sup>  
11 The trend in current literature is to report exceptional enhancement factors, and the  
12 rest of the components of the performance vector are seldom analyzed. These often  
13 neglected factors are crucial in the case of real integrated biomolecule sensing  
14 systems, in which, apart from ultrahigh sensitivity, it is highly desirable to  
15 quantitatively assess the analyte concentration. This requires extremely reproducible  
16 SERS substrates, which can withstand repeated and reliable calibrations.<sup>10</sup> The  
17 approach presented here, based on low cost EISA dip coating methods, can be  
18 extended to surfaces of arbitrary shape, lab-on-chip setups, microfluidic channels  
19 and nanometric and colloidal probes.<sup>62</sup> In addition, there is still plenty of room to  
20 optimize the silver loading and interconnectivity, in order to tune the plasmons and  
21 hot spots within the mesopore system.<sup>25, 45, 48</sup> Given that the Raman signal is strongly  
22 dependent on the available Ag surface for binding 4-MP, the interconnected pores in  
23 the MOTF matrices have to fulfil a double purpose: on one hand, they provide the  
24 support for the Ag NPs, and on the other, they allow the free diffusion of  
25 analytes/reactants to reach the Ag surface. This results in a compromise between a  
26 high density of Ag metallic surfaces for anchoring 4-MP and keeping the  
27 interconnectivity in the system at maximum. Mesoporous systems have in addition  
28 the possibility to generate permselectivity, either by anchoring functional groups or  
29 polymers to the MOTF surface<sup>63-65</sup> or by using multilayers, resulting in a new  
30 generation of fully integrated chemical devices and microarray setups for complex  
31 problems such as environmental issues or proteomics.<sup>66</sup>

## 32 33 34 35 36 37 38 39 40 41 42 43 **Acknowledgements**

44 Funding was provided by CONICET (PIP 5191), ANPCyT (PICT #0026, #33973,  
45 #1848, #2087 #00392, #2012-1167 PAE 2004 22711), UBACyT (20020100100636),  
46 UNSAM (SJ10/20), CONICET (GI-PIP 11220110101020) and ABTLus for access  
47 to LNLS SAXS1 and XRD2 beamlines. G.J.A.A.S.I., A.W., H.T., A.F., M.C.F.,  
48 M.G., N.T. and S.A.B. are members of CONICET. E.D.M. acknowledges a doctoral  
49 fellowship from CONICET.

## 50 51 52 53 54 55 56 57 58 59 60 **Supporting Information**

Figures presenting structural analysis (XRR, UV-Vis), Raman spectra of 4-MP  
adsorbed onto different substrates, of other analytes, and signals of blank  
experiments, are provided. This information is available free of charge via the  
Internet at <http://pubs.acs.org/>.

## References

1. Fleischmann, M.; Hendra, P.; McQuillan, A., Raman spectra of pyridine adsorbed at a silver electrode. *Chem. Phys. Lett.* **1974**, *26* (2), 163-166.
2. Nie, S.; Emory, S. R., Probing single molecules and single nanoparticles by surface-enhanced Raman scattering. *Science* **1997**, *275* (5303), 1102-1106.
3. Baker, G. A.; Moore, D. S., Progress in plasmonic engineering of surface-enhanced Raman-scattering substrates toward ultra-trace analysis. *Anal. Bioanal. Chem.* **2005**, *382* (8), 1751-1770.
4. Kneipp, K.; Wang, Y.; Kneipp, H.; Perelman, L. T.; Itzkan, I.; Dasari, R.; Feld, M. S., Single molecule detection using surface-enhanced Raman scattering (SERS). *Phys. Rev. Lett.* **1997**, *78* (9), 1667-1670.
5. Moskovits, M., Surface-enhanced Raman spectroscopy: A brief retrospective. *J. Raman Spectrosc.* **2005**, *36* (6-7), 485-496.
6. Etchegoin, P.; Maher, R. C.; Cohen, L. F.; Hartigan, H.; Brown, R. J. C.; Milton, M. J. T.; Gallop, J. C., New limits in ultrasensitive trace detection by surface enhanced Raman scattering (SERS). *Chem. Phys. Lett.* **2003**, *375* (1-2), 84-90.
7. Jiang, J.; Bosnick, K.; Maillard, M.; Brus, L., Single molecule Raman spectroscopy at the junctions of large Ag nanocrystals. *J. Phys. Chem. B* **2003**, *107* (37), 9964-9972.
8. Markel, V. A.; Shalaev, V. M.; Zhang, P.; Huynh, W.; Tay, L.; Haslett, T. L.; Moskovits, M., Near-field optical spectroscopy of individual surface-plasmon modes in colloid clusters. *Phys. Rev. B: Condens. Matter Mater. Phys.* **1999**, *59* (16), 10903-10909.
9. Zayak, A. T.; Hu, Y. S.; Choo, H.; Bokor, J.; Cabrini, S.; Schuck, P. J.; Neaton, J. B., Chemical Raman enhancement of organic adsorbates on metal surfaces. *Phys. Rev. Lett.* **2011**, *106* (8), 083003-083006.
10. Ko, H.; Singamaneni, S.; Tsukruk, V. V., Nanostructured surfaces and assemblies as SERS media. *Small* **2008**, *4* (10), 1576-1599.
11. Jones, M. R.; Osberg, K. D.; Macfarlane, R. J.; Langille, M. R.; Mirkin, C. A., Templated techniques for the synthesis and assembly of plasmonic nanostructures. *Chem. Rev.* **2011**, *111* (6), 3736-3827.
12. Brolo, A. G.; Arctander, E.; Gordon, R.; Leathem, B.; Kavanagh, K. L., Nanohole-enhanced Raman scattering. *Nano Lett.* **2004**, *4* (10), 2015-2018.
13. Jensen, T. R.; Schatz, G. C.; Van Duyne, R. P., Nanosphere lithography: Surface plasmon resonance spectrum of a periodic array of silver nanoparticles by ultraviolet - Visible extinction spectroscopy and electrodynamic modeling. *J. Phys. Chem. B* **1999**, *103* (13), 2394-2401.
14. Mahajan, S.; Abdelsalam, M.; Suguwara, Y.; Cintra, S.; Russell, A.; Baumberg, J.; Bartlett, P., Tuning plasmons on nano-structured substrates for NIR-SERS. *PCCP* **2007**, *9* (1), 104-109.
15. Wang, H.; Levin, C. S.; Halas, N. J., Nanosphere arrays with controlled sub-10-nm gaps as surface-enhanced Raman spectroscopy substrates. *J. Am. Chem. Soc.* **2005**, *127* (43), 14992-14993.
16. Lee, S. J.; Morrill, A. R.; Moskovits, M., Hot spots in silver nanowire bundles for surface-enhanced Raman spectroscopy. *J. Am. Chem. Soc.* **2006**, *128* (7), 2200-2201.
17. Wu, Y.; Livneh, T.; Zhang, Y. X.; Cheng, G.; Wang, J.; Tang, J.; Moskovits, M.; Stucky, G. D., Templated synthesis of highly ordered mesostructured nanowires and nanowire arrays. *Nano Lett.* **2004**, *4* (12), 2337-2342.
18. Wang, X.; Li, M.; Meng, L.; Lin, K.; Feng, J.; Huang, T.; Yang, Z.; Ren, B., Probing the location of hot spots by Surface-Enhanced Raman Spectroscopy: Toward uniform substrates. *ACS Nano* **2014**, *8* (1), 528-536.
19. Brown, R. J. C.; Milton, M. J. T., Nanostructures and nanostructured substrates for surface-enhanced Raman scattering (SERS). *J. Raman Spectrosc.* **2008**, *39* (10), 1313-1326.
20. López-Puente, V.; Abalde-Cela, S.; Angelomé, P. C.; Alvarez-Puebla, R. A.; Liz-Marzán, L. M., Plasmonic mesoporous composites as molecular sieves for SERS detection. *J. Phys. Chem. Lett.* **2013**, *4* (16), 2715-2720.
21. Malfatti, L.; Falcaro, P.; Marmioli, B.; Amenitsch, H.; Piccinini, M.; Falqui, A.; Innocenzi, P., Nanocomposite mesoporous ordered films for lab-on-chip intrinsic surface enhanced Raman scattering detection. *Nanoscale* **2011**, *3* (9), 3760-3766.
22. Mura, S.; Greppi, G.; Innocenzi, P.; Piccinini, M.; Figus, C.; Marongiu, M. L.; Guo, C.; Irudayaraj, J., Nanostructured thin films as surface-enhanced Raman scattering substrates. *J. Raman Spectrosc.* **2013**, *44* (1), 35-40.

- 1  
2  
3 23. Sugikawa, K.; Nagata, S.; Furukawa, Y.; Kokado, K.; Sada, K., Stable and Functional Gold Nanorod  
4 Composites with a Metal-Organic Framework Crystalline Shell. *Chem. Mater.* **2013**, *25* (13), 2565-2570.
- 5 24. Fuertes, M. C.; Marchena, M.; Marchi, M. C.; Wolosiuk, A.; Soler-Illia, G. J. A. A., Controlled deposition of  
6 silver nanoparticles in mesoporous single- Or multilayer thin films: From tuned pore filling to selective spatial  
7 location of nanometric objects. *Small* **2009**, *5* (2), 272-280.
- 8 25. Martínez, E. D.; Granja, L.; Bellino, M. G.; Soler-Illia, G. J. A. A., Electrical conductivity in patterned silver-  
9 mesoporous titania nanocomposite thin films: Towards robust 3D nano-electrodes. *PCCP* **2010**, *12* (43), 14445-  
10 14448.
- 11 26. Soler-Illia, G. J. D. A. A.; Sanchez, C.; Lebeau, B.; Patarin, J., Chemical strategies to design textured  
12 materials: From microporous and mesoporous oxides to nanonetworks and hierarchical structures. *Chem. Rev.*  
13 **2002**, *102* (11), 4093-4138.
- 14 27. Yamauchi, Y.; Momma, T.; Kitoh, H.; Osaka, T.; Kuroda, K., Fabrication of mesoporous Pt inside  
15 micrometer channels via "solvent-evaporation-mediated direct physical casting". *Electrochem. Commun.* **2005**, *7*  
16 (12), 1364-1370.
- 17 28. Yang, P.; Deng, T.; Zhao, D.; Feng, P.; Pine, D.; Chmelka, B. F.; Whitesides, G. M.; Stucky, G. D.,  
18 Hierarchically ordered oxides. *Science* **1998**, *282* (5397), 2244-2246.
- 19 29. Fuertes, M. C.; Colodrero, S.; Lozano, G.; González-Elipé, A. R.; Grosso, D.; Boissière, C.; Sánchez, C.;  
20 Soler-Illia, G. J. D. A. A.; Míguez, H., Sorption properties of mesoporous multilayer thin films. *Journal of*  
21 *Physical Chemistry C* **2008**, *112* (9), 3157-3163.
- 22 30. Yang, P.; Rizvi, A. H.; Messer, B.; Chmelka, B. F.; Whitesides, G. M.; Stucky, G. D., Patterning porous  
23 oxides within microchannel networks. *Adv. Mater.* **2001**, *13* (6), 427-431.
- 24 31. Calvo, A.; Angelomé, P. C.; Sánchez, V. M.; Scherlis, D. A.; Williams, F. J.; Soler-Illia, G. J. A. A.,  
25 Mesoporous aminopropyl-functionalized hybrid thin films with modulable surface and environment-responsive  
26 behavior. *Chem. Mater.* **2008**, *20* (14), 4661-4668.
- 27 32. Calvo, A.; Yameen, B.; Williams, F. J.; Azzaroni, O.; Soler-Illia, G. J. A. A., Facile molecular design of  
28 hybrid functional assemblies with controllable transport properties: Mesoporous films meet polyelectrolyte  
29 brushes. *Chem. Commun.* **2009**, (18), 2553-2555.
- 30 33. Angelomé, P. C.; Cecilia Fuertes, M.; Soler-Illia, G. J. A. A., Multifunctional, multilayer, multiscale:  
31 Integrative synthesis of complex macroporous and mesoporous thin films with spatial separation of porosity and  
32 function. *Adv. Mater.* **2006**, *18* (18), 2397-2402.
- 33 34. Fuertes, M. C.; López-Alcaraz, F. J.; Marchi, M. C.; Troiani, H. E.; Luca, V.; Míguez, H.; Soler-Illia, G. J. D.  
34 A. A., Photonic crystals from ordered mesoporous thin-film functional building blocks. *Adv. Funct. Mater.* **2007**,  
35 *17* (8), 1247-1254.
- 36 35. Zelcer, A.; Wolosiuk, A.; Soler-Illia, G. J. A. A., Carbonaceous submicron sized islands: A surface patterning  
37 route to hierarchical macro/mesoporous thin films. *J. Mater. Chem.* **2009**, *19* (24), 4191-4196.
- 38 36. Crepaldi, E. L.; Soler-Illia, G. J. D. A. A.; Grosso, D.; Cagnol, F.; Ribot, F.; Sanchez, C., Controlled  
39 formation of highly organized mesoporous titania thin films: From mesostructured hybrids to mesoporous  
40 nanoanatase TiO<sub>2</sub>. *J. Am. Chem. Soc.* **2003**, *125* (32), 9770-9786.
- 41 37. Sanchez, C.; Boissière, C.; Grosso, D.; Laberty, C.; Nicole, L., Design, synthesis, and properties of inorganic  
42 and hybrid thin films having periodically organized nanoporosity. *Chem. Mater.* **2008**, *20* (3), 682-737.
- 43 38. Attard, G. S.; Bartlett, P. N.; Coleman, N. R. B.; Elliott, J. M.; Owen, J. R.; Wang, J. H., Mesoporous  
44 platinum films from lyotropic liquid crystalline phases. *Science* **1997**, *278* (5339), 838-840.
- 45 39. Pérez, M. D.; Otal, E.; Bilmes, S. A.; Soler-Illia, G. J. A. A.; Crepaldi, E. L.; Grosso, D.; Sanchez, C.,  
46 Growth of gold nanoparticle arrays in TiO<sub>2</sub> mesoporous matrixes. *Langmuir* **2004**, *20* (16), 6879-6886.
- 47 40. Besson, S.; Gacoin, T.; Ricolleau, C.; Boilot, J. P., Silver nanoparticle growth in 3D-hexagonal mesoporous  
48 silica films. *Chem. Commun.* **2003**, *9* (3), 360-361.
- 49 41. Huang, M. H.; Choudrey, A.; Yang, P., Ag nanowire formation within mesoporous silica. *Chem. Commun.*  
50 **2000**, (12), 1063-1064.
- 51 42. Kumai, Y.; Tsukada, H.; Akimoto, Y.; Sugimoto, N.; Seno, Y.; Fukuoka, A.; Ichikawa, M.; Inagaki, S.,  
52 Highly ordered platinum nanodot arrays with cubic symmetry in mesoporous thin films. *Adv. Mater.* **2006**, *18*  
53 (6), 760-762.
- 54 43. Wright, A.; Gabaldon, J.; Burckel, D. B.; Jiang, Y. B.; Tian, Z. R.; Liu, J.; Brinker, C. J.; Fan, H.,  
55 Hierarchically organized nanoparticle mesostructure arrays formed through hydrothermal self-assembly. *Chem.*  
56 *Mater.* **2006**, *18* (13), 3034-3038.
- 57  
58  
59  
60



- 1  
2  
3  
4  
5  
6  
7  
8  
9  
10  
11  
12  
13  
14  
15  
16  
17  
18  
19  
20  
21  
22  
23  
24  
25  
26  
27  
28  
29  
30  
31  
32  
33  
34  
35  
36  
37  
38  
39  
40  
41  
42  
43  
44  
45  
46  
47  
48  
49  
50  
51  
52  
53  
54  
55  
56  
57  
58  
59  
60
44. Bronstein, L., Nanoparticles Made in Mesoporous Solids. In *Colloid Chemistry I*, Antonietti, M., Ed.; Springer Berlin Heidelberg: 2003; Chapter 3, pp 55-89.
45. Martíñez, E. D.; Bellino, M. G.; Soler-Illia, G. J. A. A., Patterned production of silver-mesoporous titania nanocomposite thin films using lithography-assisted metal reduction. *ACS Applied Materials and Interfaces* **2009**, *1* (4), 746-749.
46. Koura, N., Electroless Plating of Silver. In *Electroless Plating: Fundamentals and Applications*, Mallory, G. O.; Hajdu, J. B., Eds.; American Electroplaters and Surface Finishers Society: Orlando, FL, 1990; Chapter 17, pp 441-462.
47. Boissiere, C.; Grosso, D.; Lepoutre, S.; Nicole, L.; Bruneau, A. B.; Sanchez, C., Porosity and mechanical properties of mesoporous thin films assessed by environmental ellipsometric porosimetry. *Langmuir* **2005**, *21* (26), 12362-71.
48. Sánchez, V. M.; Martínez, E. D.; Martínez Ricci, M. L.; Troiani, H.; Soler-Illia, G. J. A. A., Optical properties of Au nanoparticles included in mesoporous TiO<sub>2</sub> thin films: A dual experimental and modeling study. *Journal of Physical Chemistry C* **2013**, *117* (14), 7246-7259.
49. Gibaud, A.; Dourdain, S.; Vignaud, G., Analysis of mesoporous thin films by X-ray reflectivity, optical reflectivity and grazing incidence small angle X-ray scattering. *Appl. Surf. Sci.* **2006**, *253* (1 SPEC. ISS.), 3-11.
50. Baldwin, J. A.; Vlčková, B.; Andrews, M. P.; Butler, I. S., Surface-enhanced raman scattering of mercaptopyrindines and pyrazinamide incorporated in silver colloid-adsorbate films. *Langmuir* **1997**, *13* (14), 3744-3751.
51. Tognalli, N.; Fainstein, A.; Calvo, E.; Bonazzola, C.; Pietrasanta, L.; Campoy-Quiles, M.; Etchegoin, P., SERS in PAH-Os and gold nanoparticle self-assembled multilayers. *J. Chem. Phys.* **2005**, *123* (4), 044707.
52. Jain, P. K.; El-Sayed, M. A., Plasmonic coupling in noble metal nanostructures. *Chem. Phys. Lett.* **2010**, *487* (4-6), 153-164.
53. Ung, T.; Liz-Marzán, L. M.; Mulvaney, P., Optical properties of thin films of AuO/SiO<sub>2</sub> particles. *J. Phys. Chem. B* **2001**, *105* (17), 3441-3452.
54. Jiang, X.; Yang, M.; Meng, Y.; Jiang, W.; Zhan, J., Cysteamine-modified silver nanoparticle aggregates for quantitative SERS sensing of pentachlorophenol with a portable Raman spectrometer. *ACS applied materials & interfaces* **2013**, *5* (15), 6902-8.
55. Norrod, K. L.; Sudnik, L. M.; Rousell, D.; Rowlen, K. L., Quantitative comparison of five SERS substrates: Sensitivity and limit of detection. *Appl. Spectrosc.* **1997**, *51* (7), 994-1001.
56. Sudnik, L. M.; Norrod, K. L.; Rowlen, K. L., SERS-active Ag films from photoreduction of Ag<sup>+</sup> on TiO<sub>2</sub>. *Appl. Spectrosc.* **1996**, *50* (3), 422-424.
57. Henglein, A., Colloidal Silver Nanoparticles: Photochemical preparation and interaction with O<sub>2</sub>, CCl<sub>4</sub>, and some metal ions. *Chem. Mater.* **1998**, *10* (1), 444-450.
58. Angelomé, P. C.; Andrini, L.; Calvo, M. E.; Requejo, F. G.; Bilmes, S. A.; Soler-Illia, G. J. A. A., Mesoporous anatase TiO<sub>2</sub> films: Use of Ti K XANES for the quantification of the nanocrystalline character and substrate effects in the photocatalysis behavior. *Journal of Physical Chemistry C* **2007**, *111* (29), 10886-10893.
59. Yu, J.; Zhao, X., Effect of substrates on the photocatalytic activity of nanometer TiO<sub>2</sub> thin films. *Mater. Res. Bull.* **2000**, *35* (8), 1293-1301.
60. Pierre, M. C. S.; Haes, A. J., Purification implications on SERS activity of silica coated gold nanospheres. *Anal. Chem.* **2012**, *84* (18), 7906-7911.
61. Soler-Illia, G. J. A. A.; Angelome, P. C.; Fuertes, M. C.; Calvo, A.; Wolosiuk, A.; Zelcer, A.; Bellino, M. G.; Martínez, E. D., Mesoporous hybrid and nanocomposite thin films. A sol-gel toolbox to create nanoconfined systems with localized chemical properties. *J. Sol-Gel Sci. Technol.* **2012**, *57* (3), 299-312.
62. Scodeller, P.; Flexer, V.; Szamocki, R.; Calvo, E. J.; Tognalli, N.; Troiani, H.; Fainstein, A., Wired-enzyme core-shell Au nanoparticle biosensor. *J. Am. Chem. Soc.* **2008**, *130* (38), 12690-12697.
63. Calvo, A.; Yameen, B.; Williams, F. J.; Soler-Illia, G. J. A. A.; Azzaroni, O., Mesoporous films and polymer brushes helping each other to modulate ionic transport in nanoconfined environments. An interesting example of synergism in functional hybrid assemblies. *J. Am. Chem. Soc.* **2009**, *131* (31), 10866-10868.
64. Fattakhova-Rohlfing, D.; Wark, M.; Rathouský, J., Ion-permselective pH-switchable mesoporous silica thin layers. *Chem. Mater.* **2007**, *19* (7), 1640-1647.
65. Taffa, D. H.; Kathiresan, M.; Walder, L.; Seelandt, B.; Wark, M., Pore size and surface charge control in mesoporous TiO<sub>2</sub> using post-grafted SAMs. *PCCP* **2010**, *12* (7), 1473-1482.

1  
2  
3 66. Mahajan, S.; Richardson, J.; Brown, T.; Bartlett, P. N., SERS-melting: A new method for discriminating  
4 mutations in DNA sequences. *J. Am. Chem. Soc.* **2008**, *130* (46), 15589-15601.  
5  
6  
7  
8  
9  
10  
11  
12  
13  
14  
15  
16  
17  
18  
19  
20  
21  
22  
23  
24  
25  
26  
27  
28  
29  
30  
31  
32  
33  
34  
35  
36  
37  
38  
39  
40  
41  
42  
43  
44  
45  
46  
47  
48  
49  
50  
51  
52  
53  
54  
55  
56  
57  
58  
59  
60

## Table Of Contents Figure

